Modified saddle-point method applied to high-order above-threshold ionization and high-order harmonic generation: Slater-type versus asymptotic ground-state wave function

A. S. Jašarević,[1] E. Hasović,[1] and D. B. Milošević[1,2]

[1]*University of Sarajevo, Faculty of Science, Zmaja od Bosne 35, 71000 Sarajevo, Bosnia and Herzegovina*

[2]*Academy of Sciences and Arts of Bosnia and Herzegovina, Bistrik 7, 71000 Sarajevo, Bosnia and Herzegovina*

(Received 19 February 2024; accepted 8 April 2024; published 22 April 2024)

We present a modified saddle-point method and apply it to the high-order above-threshold ionization (HATI) and high-order harmonic generation (HHG) processes. When we use the Slater-type orbitals to describe the ground-state wave function of the valence electron in a noble gas atom, we cannot apply the ordinary saddle-point method (SPM) because the singular points of the ionization matrix element, as well as the recombination matrix element for HHG, are in the vicinity of the corresponding saddle points. Therefore, we present a modification of the SPM and show that the obtained results are in excellent agreement with the spectra calculated by numerical integration. Furthermore, we compare the results obtained by the modified SPM with those obtained by the ordinary SPM with the asymptotic ground-state wave function. We conclude that both methods work for HATI, but for HHG we show that it is necessary to use the modified SPM because the recombination happens close to the atomic core, where the electron ground state is well described only by the Slater-type orbitals.

DOI: 10.1103/PhysRevA.109.043114

I. INTRODUCTION

Since the early days of lasers, advances in nonlinear optics have been closely linked to the quest for shorter laser pulses. These efforts have led to our ability to observe and manipulate the behavior of electrons in atoms and molecules with attosecond pulses—the shortest pulses currently available [1–5]. To generate, separate, and analyze attosecond pulses, it is essential to understand the interaction between strong laser fields and matter. In the field of ultrafast laser-matter interactions, the phenomena of above-threshold ionization (ATI) [2,6–9] and high-order harmonic generation (HHG) [6,10–12] are processes that have been studied with particular attention. The attempts to describe these phenomena have led to the development and application of various theoretical frameworks. Among these, the saddle-point method (SPM) proves to be a powerful and versatile tool that provides valuable insights into the interaction between intense laser fields and matter.

In the ATI process, an atom or molecule is ionized in the presence of a strong laser field, whereby more photons are absorbed from the laser field than are required for ionization. For certain laser-field configurations, the liberated electron can be compelled back toward its parent ion by the laser field. Should this electron recombine with the ion, its entire energy is emitted during the HHG process as a single high-energy photon. In addition, the returning electron can elastically scatter off the parent ion and move toward the detector with a higher energy. This process is called high-order ATI (HATI). The presented model for both HHG and HATI is called the three-step model [13,14]. Both processes can be theoretically described by a semiclassical theory based on the strong-field approximation (SFA) [2,6,15–17]. Within the SFA, the transition amplitude of HHG and HATI processes can be represented by a multidimensional integral over ionization time, recombination (rescattering) time, and the canonical momentum between ionization and recombination (rescattering). Since the integrating function can be written as a product $h(z)\exp[iS(z)]$, where $h(z)$ and $S(z)$ are complex analytic functions of the complex variable z, the transition amplitude of HHG and HATI can be calculated by solving the five-dimensional integral using the SPM. Within the SPM, one has to find complex solutions z_s of the saddle-point (SP) equation $dS/dz = 0$ and then expand the functions $h(z)$ and $S(z)$ around these SP solutions. The corresponding integral can be then approximated by the sum of the contributions of the SP solutions.

The SP solutions for ATI induced by various laser fields have been analyzed in detail in Ref. [18]. For a linearly polarized laser field the classification of the SP solutions and analysis of the corresponding quantum trajectories (orbits) has been presented in Ref. [19] for HHG and in Refs. [20,21] for HATI. The case of an elliptically polarized field has been analyzed in Refs. [22–24], while the bicircular and orthogonally polarized two-color fields were considered in Refs. [25–27] and [28,29], respectively.

In the present paper we consider the application of the SPM to HHG and HATI processes, where the ground-state wave function of the valence electron is modeled as an asymptotic or as a Slater-type orbital (STO) wave function (by the STO wave function we mean that it is given as a linear combination of the STOs). If we use the asymptotic wave function, then the ionization and recombination matrix elements are singular at the saddle points. The singularity problem was solved earlier [30] and the SPM was applied to HATI [2,26] and HHG [27]. On the other hand, if we use the STO as the ground-state wave function, the ionization and recombination matrix elements are not exactly singular at the saddle points, but the singular points are very close to the saddle points. Since

the direct application of the SPM is not possible in this case, we introduced a modification of the SPM based on the expansion of the ionization matrix element in the Laurent series around each singular point and applied it to ATI [31]. In the present paper we apply this modified SPM to analyze HATI and HHG spectra for a linearly polarized laser field. We find excellent agreement between the spectra obtained using the modified SPM and those obtained by the numerical integration of the T-matrix element, and conclude that it is appropriate to use the modified SPM in the analysis of the HHG process. We use atomic system of units.

II. THEORY

A. Improved strong-field approximation for HATI and HHG

The quantum-mechanical treatment of the above-mentioned three-step model is based on the improved strong-field approximation (ISFA) [2,6,26]. The ISFA assumes that the electron released in the HATI (HHG) process interacts with the parent ion only during ionization and rescattering (recombination), while the interaction with the parent ion during propagation is neglected. For both processes, the T-matrix element can be written in the form [6,15–17,26]

$$T_m^P(n) = -\frac{i}{T}\int_0^T dt \int d\mathbf{k} \int_{-\infty}^{t} dt_0\, e^{iS_P(\mathbf{k};t,t_0)} \times \mathcal{M}_P(\mathbf{k};t)\langle \mathbf{k}+\mathbf{A}(t_0)|\mathbf{r}\cdot\mathbf{E}(t_0)|\psi_{lm}\rangle, \quad (1)$$

where n is the number of absorbed laser field photons having the angular frequency ω, $T = 2\pi/\omega$ is the period of the laser field, and P denotes the process (HATI or HHG), while t_0 is the moment of ionization, t the moment of rescattering (recombination), $\mathbf{k}$ the canonical momentum between the ionization and rescattering (recombination), and $\mathbf{E}(t) = -\dot{\mathbf{A}}(t)$ the electric field vector, with $\mathbf{A}(t)$ being the vector potential. For HHG the number of absorbed photons n is equal to the harmonic order, while for HATI the energy conservation condition is $n\omega = E_\mathbf{p} + I_p + U_p$, where $E_\mathbf{p}$ is the emitted photoelectron energy, I_p is the atomic ionization potential, and U_p is the ponderomotive energy of the electron in the laser field [26].

In Eq. (1) $\langle \mathbf{k}+\mathbf{A}(t_0)|\mathbf{r}\cdot\mathbf{E}(t_0)|\psi_{lm}\rangle$, with ψ_{lm} the ground-state wave function characterized by the orbital quantum number l and the magnetic quantum number m, is the ionization matrix element, while $\mathcal{M}_P(\mathbf{k};t)$ represents the rescattering (recombination) matrix element in the case of HATI (HHG). The rescattering matrix element in the first Born approximation does not depend on the time t and is given by

$$\mathcal{M}_{\mathrm{HATI}}(\mathbf{k};t) \equiv \mathcal{M}_\mathbf{p}(\mathbf{k}) = \langle \mathbf{p}|V(\mathbf{r})|\mathbf{k}\rangle, \quad (2)$$

where $\mathbf{p}$ is the final momentum of electron. By using the double Yukawa potential [32]

$$V(\mathbf{r}) = -\frac{Z}{H}\frac{e^{-r/D}}{r}[1+(H-1)e^{-Hr/D}], \quad (3)$$

with $H = DZ^{0.4}$, where Z is the atomic number (for the neon atom $Z = 10$ and $D = 0.500$), we easily derive the rescattering matrix element (2), which is given by

$$\mathcal{M}_\mathbf{p}(\mathbf{k}) = -\frac{Z}{2\pi^2 H}\left[\frac{1}{\mathbf{K}^2+D^{-2}} + \frac{H-1}{\mathbf{K}^2+\left(\frac{H+1}{D}\right)^2}\right], \quad (4)$$

with $\mathbf{K} = \mathbf{p}-\mathbf{k}$. The recombination matrix element in the case of HHG is given by

$$\mathcal{M}_{\mathrm{HHG}}(\mathbf{k};t) \equiv \mathcal{M}_j(\mathbf{k};t) = \langle \psi_{lm}|j|\mathbf{k}+\mathbf{A}(t)\rangle, \quad (5)$$

where $j = x, y$ defines the polarization axis of the harmonic field. Both the ionization and recombination matrix elements can be obtained directly from the dipole matrix element $\langle \mathbf{k}+\mathbf{A}(t)|\mathbf{r}|\psi_{lm}\rangle$, derived in the Appendix. The modified actions $S_P(\mathbf{k};t,t_0)$ for HATI and HHG processes can be written as

$$\begin{aligned} S_{\mathrm{HATI}}(\mathbf{k};t,t_0) &= S_\mathbf{p}(t) - S_\mathbf{k}(t) + S_\mathbf{k}(t_0) + I_p t_0, \\ S_{\mathrm{HHG}}(\mathbf{k};t,t_0) &= n\omega t - S_\mathbf{k}(t) + S_\mathbf{k}(t_0) - I_p(t-t_0), \end{aligned} \quad (6)$$

with $S_\mathbf{p}(t) = \int^t dt'[\mathbf{p}+\mathbf{A}(t')]^2/2$.

In the case of HATI, the physically measurable (observable) quantity is the differential ionization rate (averaged over all possible values of m), defined as

$$\bar{w}_\mathbf{p}(n) = 4\pi p \sum_{m=-l}^{l} \left|T_{m,\mathbf{p}}^{\mathrm{HATI}}(n)\right|^2, \quad (7)$$

where we added the subscript $\mathbf{p}$ in the T-matrix element to denote the final electron momentum, with $p = |\mathbf{p}|$. For HHG the T-matrix elements are summed coherently [33] and the physically measurable quantity is the intensity of the nth harmonic

$$I_n = \frac{(n\omega)^4}{2\pi c^3}\sum_{j=x,y}\left|\sum_{m=-l}^{l} T_{m,j}^{\mathrm{HHG}}(n)\right|^2, \quad (8)$$

where subscript j in the T-matrix element denotes the polarization axis of the emitted harmonic.

B. Saddle-point method treatment

In order to find the differential ionization rate in the HATI process or the intensity of the nth harmonic in the HHG process, the SPM can be applied. The saddle-point-method approximation is performed when one deals with highly oscillatory integrals of the form $\int_\Gamma dz\, h(z)\exp[iS(z)]$, where $h(z)$ and $S(z)$ are complex analytic functions of the complex variable z. In the SP approximation, the contour of the integration Γ is deformed so that it passes through the saddle points z_s which are solutions of the SP equation $S'(z_s) = 0$ (see Ref. [18] and references therein). The main contributions to the integral come from small neighbourhoods around these saddle points. If the function $h(z)$ does not change too much around the saddle points z_s it can be approximated by its value at the saddle point $h(z_s)$ and our integral can be approximated as [34–39]

$$\int_\Gamma dz\, h(z)e^{iS(z)} \approx \sum_s \sqrt{\frac{2\pi i}{S''(z_s)}}h(z_s)e^{iS(z_s)}. \quad (9)$$

The usual treatment of HATI and HHG (see Refs. [26,27,29]) is to first apply the SPM to the integrals

$\int_0^T dt \int d\mathbf{k}$ in the T-matrix element (1) and then to the integral $\int_{-\infty}^{t} dt_0$. The triple integral over $d\mathbf{k}$ results in the factor $\{2\pi/[i(t-t_0)]\}^{3/2}$ with the corresponding SP solution

$$\mathbf{k}_{\rm st} = -\frac{\boldsymbol{\alpha}(t) - \boldsymbol{\alpha}(t_0)}{t - t_0}, \tag{10}$$

where $\boldsymbol{\alpha}(t) = \int^t dt' \mathbf{A}(t')$. Physically, Eq. (10) represents the return condition of the electron to the parent ion. The integral over dt gives the factor $(2\pi i/S''_{P,s})^{1/2}$, where $S''_{P,s} = \partial^2 S_P(\mathbf{k}_{\rm st}; t, t_0)/\partial t^2|_{t=t_s}$, while t_s are solutions of the SP equation $\partial S_P(\mathbf{k}_{\rm st}; t, t_0)/\partial t = 0$. For HATI we obtain

$$S''_{{\rm HATI},s} = (\mathbf{k}_{\rm st} - \mathbf{p}) \cdot \mathbf{E}(t_s) + \frac{[\mathbf{k}_{\rm st} + \mathbf{A}(t_s)]^2}{t_s - t_0}, \tag{11}$$

with the saddle-point equation

$$\tfrac{1}{2}[\mathbf{k}_{\rm st} + \mathbf{A}(t_s)]^2 = \tfrac{1}{2}[\mathbf{p} + \mathbf{A}(t_s)]^2, \tag{12}$$

while for HHG we can write

$$S''_{{\rm HHG},s} = [\mathbf{k}_{\rm st} + \mathbf{A}(t_s)] \cdot \mathbf{E}(t_s) + \frac{[\mathbf{k}_{\rm st} + \mathbf{A}(t_s)]^2}{t_s - t_0}, \tag{13}$$

with the corresponding SP equation

$$\tfrac{1}{2}[\mathbf{k}_{\rm st} + \mathbf{A}(t_s)]^2 = n\omega - I_p. \tag{14}$$

Equations (12) and (14) represent the energy conservation conditions at the moment of rescattering and recombination, respectively. The T-matrix element now takes the form

$$T_m^{P,{\rm SP}}(n) = \frac{2^{3/2}\pi^2}{iT} \sum_{t_s} \int_{-\infty}^{t_s} dt_0 \frac{\mathcal{M}_P(\mathbf{k}_{\rm st}; t_s)}{[i(t_s - t_0)]^{3/2}} \left(\frac{2i}{S''_{P,s}}\right)^{1/2} \times \langle \mathbf{k}_{\rm st} + \mathbf{A}(t_0) | \mathbf{r} \cdot \mathbf{E}(t_0) | \psi_{lm} \rangle e^{iS_P(\mathbf{k}_{\rm st}; t_s, t_0)}. \tag{15}$$

The SP treatment of the integral over dt_0 is a little more complicated. The SP equation $\partial S_P(\mathbf{k}_{\rm st}; t_s, t_0)/\partial t_0 = 0$ for saddle points t_{0s} is the same for HATI and HHG, and has the form

$$\tfrac{1}{2}[\mathbf{k}_{\rm st} + \mathbf{A}(t_{0s})]^2 = -I_p, \tag{16}$$

which represents the energy conservation condition at the moment of ionization. However, the ionization matrix element $\langle \mathbf{q}_{0s} | \mathbf{r} \cdot \mathbf{E}(t_0) | \psi_{lm} \rangle$, with $\mathbf{q}_{0s} = \mathbf{k}_{\rm st} + \mathbf{A}(t_{0s})$, either diverges at the saddle points if we use the asymptotic wave function as the ground-state function ψ_{lm} [see Eq. (A11) with (A10)], or it has singular points very close to the saddle points if we use a linear combination of STOs as the ground-state wave function. The latter can be seen from Eq. (A19) by comparing the values of the coefficients ζ_i^2 with $2I_p$.

However, the asymptotic ground-state wave function describes only the behavior of the electron far from the nucleus of an atom, while the STO ground-state wave function describes the electron's behavior both near and far from the atomic nucleus. In Fig. 1 we have plotted the logarithm of the electron probability density $\rho(\mathbf{r}) = |\psi_0(\mathbf{r})|^2$, with $\psi_0 \equiv \psi_{lm}$, as a function of the distance from the nucleus (we have limited ourselves to the x axis only), for the neon atom with $l = 1$ and $m = 1$, using the STO (red solid line) and the asymptotic (black dashed line) ground-state wave function. We can see that for x larger than 2.5 a.u. the asymptotic wave function

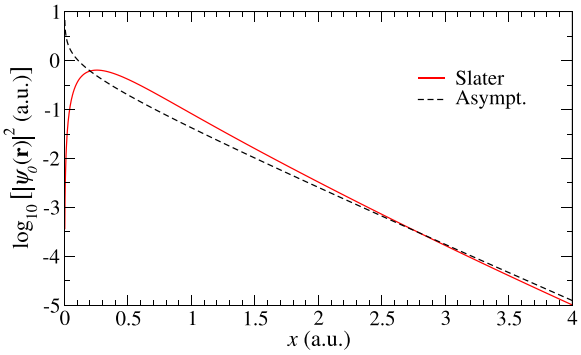

FIG. 1. Logarithm of the electron probability density $\rho(\mathbf{r}) = |\psi_0(\mathbf{r})|^2$ (in a.u.) as a function of the distance from the nucleus on the x axis, for the neon atom with $l = 1$ and $m = 1$, obtained using the STO ground-state wave function (red solid line) and the asymptotic ground-state wave function (black dashed line).

almost coincides with the STO wave function. However, in the vicinity of the atomic nucleus the two wave functions differ significantly. This will have a particular impact on the HHG rate because it contains the recombination matrix element $\langle \psi_{lm} | j | \mathbf{k}_{\rm st} + \mathbf{A}(t_s) \rangle$ and because the SP equations imply that the recombination occurs very close to the center of the atom. For more detailed analyses of the initial-state wave-functions effects in (H)ATI and HHG spectra of anions and noble gases see Refs. [40–42].

The problem with the ordinary SPM that arises when we use the STO ground-state wave functions is that, due to the proximity of the singular points to the saddle points, we cannot assume that the subintegral function does not change too much around the saddle points, and therefore we cannot use the formula (9). In the following we separately present application (modification) of the SPM in order to solve problems that arise in the case of asymptotic (STO) ground-state wave functions.

1. SPM for the case of overlapping saddle points and singular points

For the case of asymptotic ground-state wave functions the subintegral function diverges at the saddle points, and formula (9) is not applicable. The problem was solved in Ref. [30] using the formula (see also Refs. [18,43,44])

$$\int_\Gamma dz \frac{e^{iS(z)}}{[S'(z)]^\nu} \approx i^\nu \frac{\Gamma(\nu/2)}{2\Gamma(\nu)} \sqrt{\frac{2\pi i}{S''(z_0)}} \left[\frac{2}{iS''(z_0)}\right]^{\frac{\nu}{2}} e^{iS(z_0)}, \tag{17}$$

where $\Gamma(\nu)$ is the Gamma function. In order to obtain the desired form in Eq. (15), the first line is approximated by its value at t_{0s} (this is justified because it does not change too much around t_{0s}). Then, the integral of the factor in the second line of Eq. (15), after a partial integration, becomes

$$\int_{-\infty}^{t_s} dt_0 \, \langle \mathbf{q}(t_0) | \mathbf{r} \cdot \mathbf{E}(t_0) | \psi_{lm} \rangle e^{iS_P(\mathbf{k}_{\rm st}; t_s, t_0)} = -\int_{-\infty}^{t_s} dt_0 \, \tilde{\psi}_{lm}(\mathbf{q}(t_0)) \left[\frac{\mathbf{q}^2(t_0)}{2} + I_p\right] e^{iS_P(\mathbf{k}_{\rm st}; t_s, t_0)}, \tag{18}$$

where $\mathbf{q}(t_0) = \mathbf{k}_{\rm st} + \mathbf{A}(t_0)$. If we now apply the formula (17) to the integral (18), we obtain the T-matrix element for the case of asymptotic ground-state wave function

$$T_m^{P,\rm SP}(n) = \frac{i}{T} A\pi^2 \kappa^\nu \nu\Gamma(\nu/2) \sum_{t_{0s},t_s} \frac{\mathcal{M}_P(\mathbf{k}_{\rm st};t_s)}{[i(t_s-t_{0s})]^{3/2}} \times \left(\frac{2i}{S''_{P,s}}\right)^{1/2} \left(\frac{2i}{S''_{P,0s}}\right)^{(\nu+1)/2} \left(\frac{q_{0s}}{i\kappa}\right)^l \times Y_{lm}(\hat{\mathbf{q}}_{0s})\, e^{iS_{P,s}}, \tag{19}$$

with $S_{P,s} = S_P(\mathbf{k}_{\rm st}; t_s, t_{0s})$ and (both for HATI and HHG)

$$S''_{P,0s} = \left.\frac{\partial^2 S_P(\mathbf{k}_{\rm st}; t_s, t_0)}{\partial t_0^2}\right|_{t_0=t_{0s}} = -\mathbf{E}(t_{0s})\cdot\mathbf{q}_{0s}. \tag{20}$$

The quantities A, κ, and ν are defined in the Appendix, $Y_{lm}(\hat{\mathbf{q}}_{0s})$ are spherical harmonics, and $\mathbf{q}_{0s} = \mathbf{q}(t_{0s})$. Since this type of the SPM treatment has been conventional so far [26,27,29], we refer to the results obtained by Eq. (19) as ordinary SPM treatment of HATI and HHG.

2. *Modified SPM for the case when saddle points and singular points are in close proximity*

The problem that arises for the STO ground-state wave function was analyzed before for the process of direct ionization (ATI) [31]. In this paper we generalize this approach and apply it to HATI and HHG. The modified SPM deals with the integrals of the form $\int_\Gamma dz\, h(z)\exp[iS(z)]$, where the function $h(z)$ has singular points Z_s very close to the saddle points z_s of $iS(z)$. The idea is to expand the function $h(z)$ in the Laurent series around the singular points Z_s (we assume that these are the poles of order k_0)

$$h(z) = \frac{a_{-k_0,s}}{(z-Z_s)^{k_0}} + \frac{a_{-(k_0-1),s}}{(z-Z_s)^{k_0-1}} + \cdots + \frac{a_{-2,s}}{(z-Z_s)^2} + \frac{a_{-1,s}}{z-Z_s} + h_{s,\rm reg}(z), \tag{21}$$

and then to integrate the principal and regular parts of the Laurent series separately. Since the entire singularity is contained in the principal part, the regular part $h_{s,\rm reg}(z)$ can be integrated using the ordinary SPM (9). Integration over the principal part leads to the integrals of the form

$$A_{-k,s} = \int_{-\infty}^{\infty} d\eta \frac{e^{-\eta^2}}{(\eta - b_s)^k}, \tag{22}$$

with $b_s = (Z_s - z_s)/\sqrt{\frac{2i}{S''(z_s)}}$, which can be calculated via the recurrence relation

$$A_{-(k+1),s} = -\frac{2}{k}[b_s A_{-k,s} + A_{-(k-1),s}], \tag{23}$$

with

$$A_{-1,s} = i\pi e^{-b_s^2}\,\mathrm{erfc}(-ib_s), \quad A_{0,s} = \sqrt{\pi}, \tag{24}$$

where $\mathrm{erfc}(z)$ is the complementary error function. Adding it all up, the initial integral in the modified SPM can be approximated by [31]

$$\int_\Gamma dz\, h(z) e^{iS(z)} \approx \sum_s \left[\sum_{k=1}^{k_0} a_{-k,s}\left[\frac{2i}{S''(z_s)}\right]^{(1-k)/2} A_{-k,s} + \sqrt{\frac{2\pi i}{S''(z_s)}} h_{s,\rm reg}(z_s)\right] e^{iS(z_s)}. \tag{25}$$

The ionization matrix element $\langle \mathbf{q}(t_0)|\mathbf{r}\cdot\mathbf{E}(t_0)|\psi_{lm}\rangle$ in the ionization integral [first line in Eq. (18)] has the role of function $h(t_0)$ and, for neon atoms described with the STO ground-state wave function, it can be written in the form [see Eq. (A19)]

$$h(t_0) = \sum_{i=1}^4 h_i(t_0) = \sum_{i=1}^4 \frac{w_i(t_0)}{[g_i(t_0)]^4}, \tag{26}$$

where $g_i(t_0) = \mathbf{q}^2(t_0) + \zeta_i^2$ and

$$\begin{aligned} w_i(t_0) &= -mC_i \frac{8\zeta_i^{7/2}}{\pi}[E_x(t_0)f_x(t_0) + E_y(t_0)f_y(t_0)], \\ f_x(t_0) &= \mathbf{q}^2(t_0) - 6q_x^2(t_0) - 6miq_x(t_0)q_y(t_0) + \zeta_i^2, \\ f_y(t_0) &= mi\mathbf{q}^2(t_0) - 6q_x(t_0)q_y(t_0) - 6miq_y^2(t_0) + mi\zeta_i^2, \end{aligned} \tag{27}$$

where the index i denotes the STOs, while the dependence on quantum numbers l and m is assumed implicitly. The function $h(t_0)$ has fourth-order poles at the points t_{0si} which satisfy the equations $g_i(t_{0si}) = 0$, i.e.,

$$[\mathbf{k}_{\rm st} + \mathbf{A}(t_{0si})]^2 = -\zeta_i^2, \quad i = 1,2,3,4. \tag{28}$$

These equations have the same form as the SP equation (16), with the only difference that $2I_p$ is replaced by ζ_i^2. Since the values of the coefficients ζ_i^2 are very close to the value of $2I_p$ (especially for the first two STOs in the case of neon atoms), the singular points t_{0si} are close to the saddle points t_{0s}. Therefore, the index s in t_{0si} denotes the saddle point which is in a close neighborhood of the singular point, while the index i denotes the STO for which the singularity occurs. Applying formula (25) to the ionization integral (18), we obtain the T-matrix element in the modified SP approximation, by using the STO ground-state wave function of neon atoms, in the following form:

$$T_m^{P,\rm MSP}(n) = \frac{2^{3/2}\pi^2}{iT} \sum_{t_{0s},t_s} \frac{\mathcal{M}_P(\mathbf{k}_{\rm st};t_s)}{[i(t_s-t_{0s})]^{3/2}} \left(\frac{2i}{S''_{P,s}}\right)^{1/2} \times e^{iS_{P,s}} \sum_{i=1}^4 \left[\sum_{k=1}^4 a_{-k,si}\left(\frac{2i}{S''_{P,0s}}\right)^{\frac{1-k}{2}} A_{-k,si} + \left(\frac{2i\pi}{S''_{P,0s}}\right)^{1/2} h_{si,\rm reg}(t_{0s})\right], \tag{29}$$

where we have added the index i to $a_{-k,si}$, $A_{-k,si}$, and $h_{si,\rm reg}(t_{0s})$ to account for all four STOs. The implicit dependence on the quantum numbers l and m is assumed by the expansion coefficients $a_{-k,si}$. For the function (26) the expansion coefficients $a_{-k,si}$ are given in Ref. [31]. We refer to the result (29) as the modified SPM treatment of HATI and HHG.

We emphasize that the algorithm for finding saddle points and singular points consists of the following steps. We first solve the system of equations

$$\tfrac{1}{2}[\mathbf{k}_{\rm st}+\mathbf{A}(t_s)]^2=\begin{cases}\tfrac{1}{2}[\mathbf{p}+\mathbf{A}(t_s)]^2, & \text{HATI},\\ n\omega-I_p, & \text{HHG},\end{cases} \tag{30}$$

$$\tfrac{1}{2}[\mathbf{k}_{\rm st}+\mathbf{A}(t_{0s})]^2=-I_p, \tag{31}$$

$$(t_s-t_{0s})\mathbf{k}_{\rm st}=\boldsymbol{\alpha}(t_{0s})-\boldsymbol{\alpha}(t_s), \tag{32}$$

to find the saddle points $\{t_{0s},t_s\}$, and then solve the equation

$$[\mathbf{k}_{\rm st}+\mathbf{A}(t_{0si})]^2=-\zeta_i^2, \tag{33}$$

for each saddle point (with the corresponding value of $\mathbf{k}_{\rm st}$) and for each STO, in order to find the singular point t_{0si} of the ionization matrix element that is in the vicinity of corresponding saddle point t_{0s}.

III. NUMERICAL RESULTS

We present HHG and HATI spectra of Ne atoms (in the initial state with the orbital quantum number $l=1$ and the magnetic quantum number m from $-l$ to l) exposed to a linearly polarized laser field, polarized in the x direction, obtained by numerical integration and by the modified SPM. By numerical integration we mean two-dimensional integration over the times t_0 and t in Eq. (1), after the integral over the momentum $\mathbf{k}$ was solved using the SPM. Our linearly polarized laser field is defined as $\mathbf{E}(t)=E_0\sin(\omega t)\hat{\mathbf{e}}_x$, with amplitude $E_0=\sqrt{I}$, where I is the intensity of the laser field. Ponderomotive energy is given by $U_p=E_0^2/(4\omega^2)$. We chose the intensity of the laser field to be $I=2\times10^{14}$ W/cm^2 and the wavelength $\lambda=1300$ nm ($\lambda=1800$ nm) for HATI (HHG), but we have checked that our method is numerically stable for a wide range of intensities and wavelengths. Numerical integration of these highly oscillatory integrals is performed using Gauss-Legendre quadrature with several thousand nodes for each integral. We perform numerical integration of the T-matrix element as well as the SPM analysis by representing the ground-state wave function in terms of STOs, but also by its asymptotic form.

The SP solutions are classified using the usual (α,β,m) notation [19,20,26,27,29,45]. The index m, defined as $m=[\mathrm{Re}\,(t_s-t_{0s})/T]$, gives the approximate length of the travel time in multiples of the laser period. For a fixed value of m, there are two pairs of solutions within one period (for a linearly polarized laser field), indexed by $\beta=1,2$. Finally, for fixed values of β and m each pair of solutions consists of two orbits with slightly different travel times. The index α distinguishes the longer orbit ($\alpha=-1$) from the shorter orbit ($\alpha=+1$). One of the two solutions of each pair has $\mathrm{Im}\,t_r<0$ and its contribution diverges after the cutoff energy and has to be discarded after the cutoff. To avoid this divergence, the uniform approximation [19,46] has to be used.

A. High-order above-threshold ionization

In Fig. 2 we present the backward-scattering (α,β,m), $m\leqslant 2$, SP solutions $\{t_{0s},t_s\}$ for the HATI process and with electron emission in the laser field direction. For each SP solution presented, the electron energy $E_{\mathbf{p}}=\mathbf{p}^2/2$ (in units of the ponderomotive energy U_p) is plotted as a function of the real part of the electron ionization time $\mathrm{Re}\,t_0$ and the rescattering time $\mathrm{Re}\,t_r$. The solutions that should be discarded after the cutoff are marked by dashed lines. For the first four pairs of SP solutions (which are the dominant ones) in Fig. 3 we show by black thick lines the ionization time t_0 in the complex plane. For each SP-solution pair we plot the corresponding four singular-point solutions by red thin lines, one for each STO. For larger values of ζ_i^2 we have a higher imaginary part

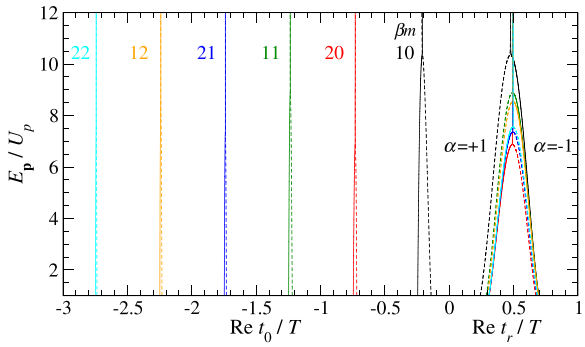

FIG. 2. SP solutions for HATI of neon atoms in a linearly polarized laser field with intensity $I=2\times10^{14}$ W/cm^2 and wavelength 1300 nm, for emission in the direction of the laser field. The dependence of the electron kinetic energy $E_{\mathbf{p}}$ (in units of ponderomotive energy U_p) on the real parts of the ionization and rescattering times t_0 and t_r is shown. Only the backward-scattering solutions with $m=0,1,2$ are presented. The indices β and m are labeled near the corresponding ionization times, while the index α is labeled near the corresponding rescattering time. The contribution of the solutions denoted by dashed lines should be discarded after the cutoff.

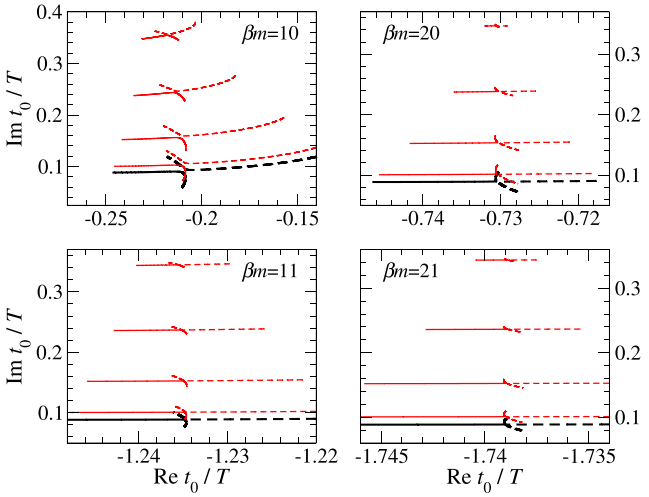

FIG. 3. Saddle-point (black thick lines) and singular-point solutions (red thin lines) in the complex plane of the ionization time for pairs of solutions $(\beta,m)=(1,0)$, $(2,0)$, $(1,1)$, and $(2,1)$, denoted in Fig. 2. For each SP solution there are four singular-point solutions, corresponding to four STOs in the wave function of the neon atom. The electron kinetic energy changes along each curve from zero to $E_{\mathbf{p}}=15U_p$. The solid and dashed curves correspond to different values of $\alpha=\pm1$ and approach each other near the cutoff of the corresponding pair.

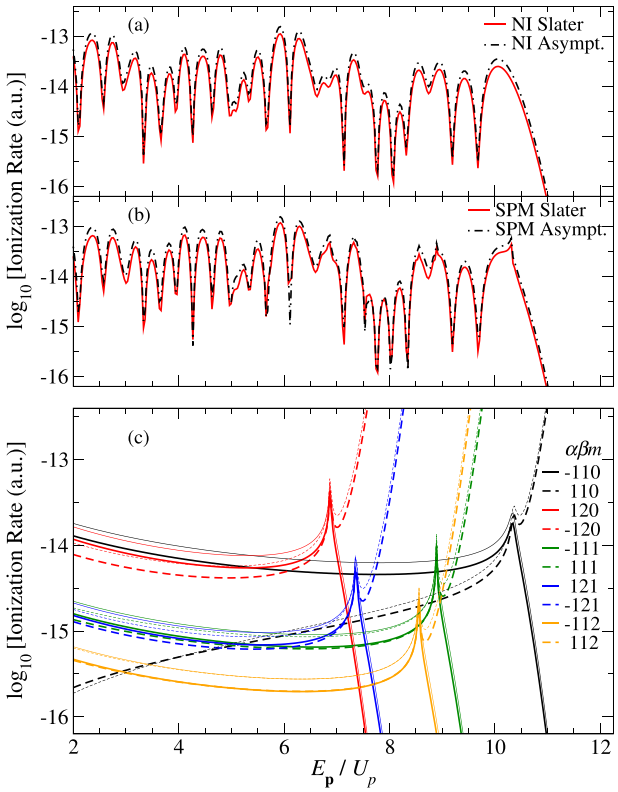

FIG. 4. Logarithm of the differential ionization rate (in a.u.) of neon atoms as a function of electron kinetic energy $E_{\mathbf{p}}$ (in units of ponderomotive energy U_p) for the same parameters as in Fig. 2. (a) Spectra obtained by numerical integration and (b) spectra obtained by the SPM. Black dot-dashed lines represent the spectra in which the asymptotic ground-state wave function is used, while the red solid lines represent the spectra in which the STO ground-state wave function is used. (c) Partial contributions of the most dominant SP solutions. Thinner lines represent contributions obtained using the asymptotic ground-state wave function, while thicker lines represent contributions obtained using the STO ground-state wave function.

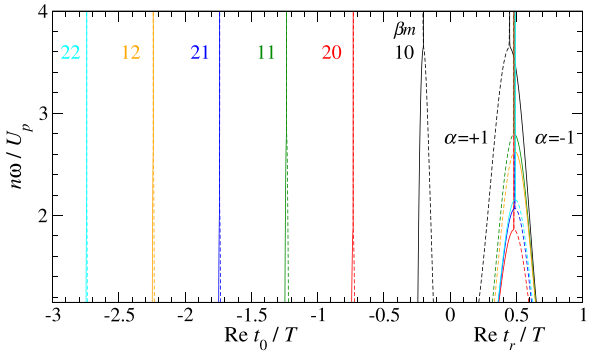

FIG. 5. Saddle-point solutions for HHG of neon atoms in a linearly polarized laser field with intensity $I = 2 \times 10^{14}$ W/cm^2 and wavelength 1800 nm. The dependence of the harmonic photon energy $n\omega$ (in units of the ponderomotive energy U_p) on the real parts of the ionization and recombination times t_0 and t_r is presented. Only the solutions with $m = 0, 1, 2$ are shown.

of the singular-point solution. It can be seen that the singular points can be close to the saddle points especially for the first two STOs.

In Fig. 4 we present the HATI spectra obtained by numerical integration [panel (a)] and by the SPM [panel (b)]. The spectra obtained using the asymptotic ground-state wave function are represented by black dot-dashed lines, while those obtained using the STO ground-state wave function are depicted by red solid lines. Since at least one singular point is very close to the saddle point, the ordinary SPM is not applicable in the case of the STO ground-state wave function, and we have to use the above-presented modified SPM. From Figs. 4(a) and 4(b), we see that the agreement between the results obtained by numerical integration and using the SPM is excellent for both the asymptotic and STO wave functions. Furthermore, it can be seen (both for the numerical integration and for the SPM) that the rates obtained using the STO ground-state wave function are lower by about a factor of two than the rates obtained using the asymptotic ground-state wave function. This difference in height of the two spectra remains constant for all energies and there is no other structural difference between these two spectra.

To explain the above-mentioned difference, in Fig. 4(c) we plot the individual contributions of the first five pairs of the SP solutions. Thinner lines represent contributions obtained using the asymptotic ground-state wave functions and formula (19), while thicker lines represent contributions obtained using the STO ground-state wave functions and formula (29). We see that for all pairs of solution the contributions obtained by the asymptotic ground-state wave function are higher than those obtained by the STO ground-state wave function. Since the rescattering matrix element, given by Eq. (4), does not depend on the ground-state wave function, the difference in height of the two spectra comes purely from the ionization matrix element. From Fig. 1 it can be seen that for the distances $x > 3$ a.u. the value of the radial part of the asymptotic wave function is higher than that of the STO wave function. Since the emission of an electron in the HATI process occurs at distances much larger than 3 a.u., the contribution to the emission rate by the ionization matrix element obtained by using the asymptotic wave functions is higher than the corresponding contribution obtained by the STO wave function. It should be noted that, by increasing the number of STOs in the ground-state wave function (we are using four orbitals from Ref. [47], while more orbitals can be found, for example, in Ref. [48]), the difference between the asymptotic and the STO wave functions will shrink at large distances, and therefore the ionization matrix element would not differ significantly for these two types of ground-state wave functions.

B. High-order harmonic generation

In Fig. 5 we present the SP solutions for the HHG process in the same way as for the HATI process. The ordinate axis now shows the harmonic photon energy $n\omega$ (in units of ponderomotive energy U_p). In Fig. 6 we show, in the complex plane, the ionization time t_0 of the first four pairs of the SP solutions (black thick lines), together with the corresponding singular-point solutions (red thin lines), for various values of the harmonic order from $n = 100$ to $n = 380$, i.e., of the

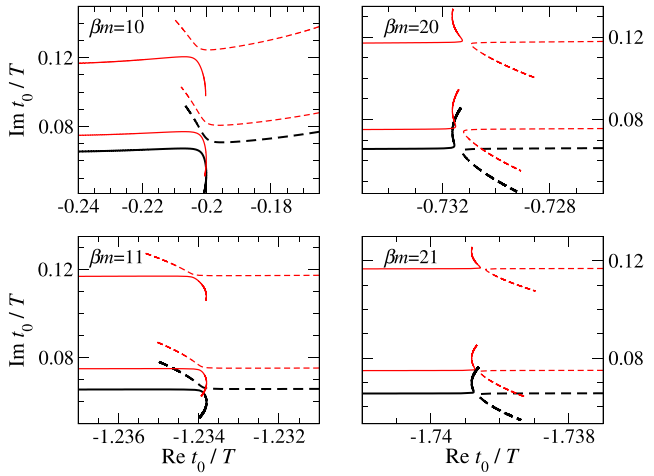

FIG. 6. Saddle-point (black thick lines) and singular-point solutions (red thin lines) in the complex plane of the ionization time for pairs of solutions $(\beta, m) = (1, 0)$, $(2, 0)$, $(1, 1)$, and $(2,1)$, denoted in Fig. 5. The results are presented similarly as in Fig. 3 for HATI, but we have shown only singular-point solutions corresponding to the first two STOs of the neon atom.

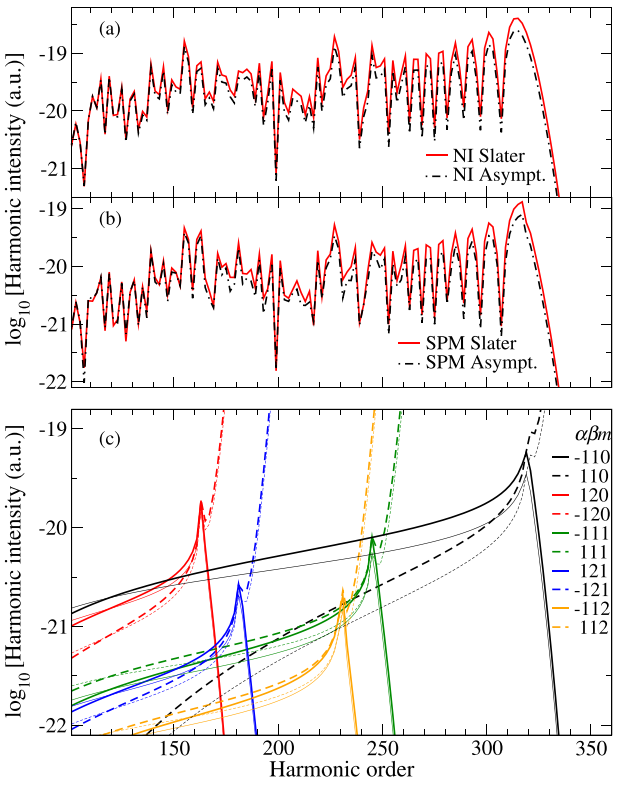

FIG. 7. Logarithm of the harmonic intensity (in a.u.) as a function of the harmonic order n for HHG of neon atoms for the same parameters as in Fig. 5. The spectra are plotted in the same way as for HATI in Fig. 4.

harmonic photon energy from $n\omega = 1.15U_p$ to $4.35U_p$. We have shown only singular-point solutions for the first two STOs. These singular-point solutions are very close to the saddle points, and one has to apply the modified SPM because application of the ordinary SPM to the HHG process will fail in this case. Singular points corresponding to the other two STOs are not shown because, as for the HATI process, they are further away from the saddle points so that the ordinary SPM, Eq. (9), would give approximately the same results as the modified SPM.

In Fig. 7 we plot the HHG spectra in the same way as for the HATI process in Fig. 4, except that the abscissa is now the harmonic order n. We see that again the agreement between the results obtained by numerical integration and using the SPM (ordinary for the asymptotic and modified for the STO wave functions) is very good. A small difference in the height of the spectra obtained by numerical integration and saddle-point methods is due to the higher-order corrections of the exponent $e^{iS(z)}$. There is again a small difference between the spectra obtained using the asymptotic and the STO wave functions, but, in contrast to the HATI case, this difference in the height of the spectra depends on the harmonic order. It is evident that the difference between the spectra increases with increasing the harmonic order. For $n < 130$ the two spectra coincide, while for $n = 315$ (near the cutoff) the difference in emission rates is by about a factor of two.

In order to explain this behavior, in Fig. 7(c) we again plot all individual contributions. It is evident that the solution pair $(\alpha, \beta, m) = (\pm 1, 1, 0)$ is dominant through the entire plateau region. For this particular pair, we can also see that the difference in the contributions obtained applying the ordinary SPM with the asymptotic wave function (thin black solid line) and applying the modified SPM with the STO wave functions (thick black solid line) increases with the increase of the harmonic order. As we have shown before for the HATI process, the difference between these two spectra can be caused by the ionization matrix element, but this difference does not depend on the electron energy or harmonic order. Therefore, we conclude that the harmonic-order dependence of the difference of the two spectra is caused only by the recombination matrix element which depends on the ground-state wave function.

Since the right-hand side of the recombination SP equation (14) is larger than zero (for higher-order harmonics such that $n\omega > I_p$), the recombination time t_r is almost real (almost, since $\mathbf{k}_{\rm st}$ is still complex), and the recombination occurs almost at the center of the atom. The difference between the STO and the asymptotic wave functions is the highest at small distances from the nucleus because the asymptotic wave function describes the ground state well only at large distances. Quantitatively, this difference can be more clearly described by considering the ground-state wave function in the momentum space $\tilde{\psi}_0(\mathbf{q})$, which is directly related to the recombination matrix element [see Eq. (A1)]. It is sufficient to consider the most dominant solution $(\alpha, \beta, m) = (-1, 1, 0)$.

In Fig. 8 we plot the dependence of the electron momentum $q_x(t) = \mathrm{Re}\,[k_{\mathrm{st},x} + A_x(t)]$ as a function of time for the dominant SP solution for two different harmonic orders $n = 51$ (black dashed line) and $n = 281$ (red solid line) from the moment of ionization $\mathrm{Re}\,t_0$ to the moment of recombination $\mathrm{Re}\,t_r$. It can be seen that the momentum of the electron at the moment of recombination for $n = 51$ ($q_{x,\mathrm{rec}} = 1.00$ a.u.) is much smaller than the momentum of the electron at the moment of recombination for $n = 281$ ($q_{x,\mathrm{rec}} = 3.56$ a.u.). If we now look

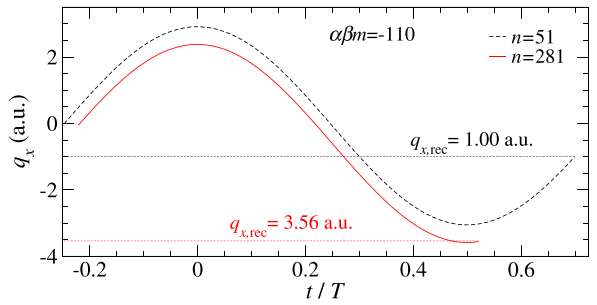

FIG. 8. Electron momentum $q_x(t) = \mathrm{Re}\,[k_{\mathrm{st},x} + A_x(t)]$ (in a.u.) as a function of time (in units of period T) for the solution $(\alpha, \beta, m) = (-1, 1, 0)$ for two different harmonic orders $n = 51$ (black dashed line) and $n = 281$ (red solid line) from the moment of ionization $\mathrm{Re}\,t_0$, to the moment of recombination $\mathrm{Re}\,t_r$. The momentum of the electron at the moment of recombination $q_{x,\mathrm{rec}} \equiv q_x(\mathrm{Re}\,t_r)$ is equal to 1.00 a.u. for $n = 51$, while for $n = 281$ it is equal to 3.56 a.u.

at Fig. 9(a), where we have plotted the logarithm of $|\tilde{\psi}_0(\mathbf{q})|^2$ as a function of the electron momentum (we have restricted ourselves to the q_x axis only) for the STO ground-state wave function (red solid line) and the asymptotic ground-state wave function (black dashed line), we can see that the difference between the two ground-state wave functions is much larger for

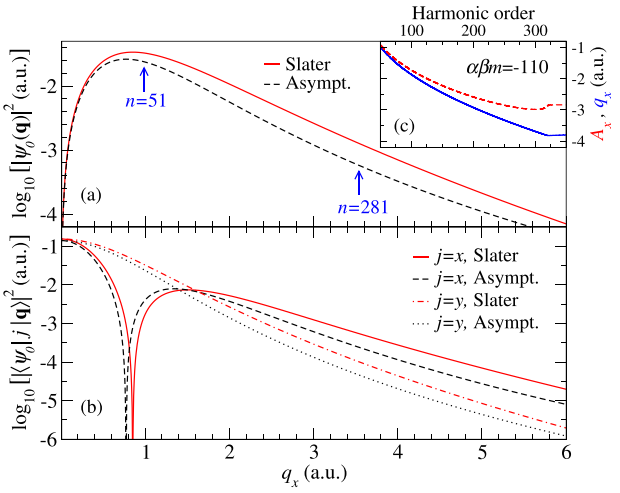

FIG. 9. Logarithm of (a) electron probability density in momentum space $|\tilde{\psi}_0(\mathbf{q})|^2$ (in a.u.) and (b) absolute square of the recombination matrix element $\langle\psi_0|j|\mathbf{k} + \mathbf{A}(t)\rangle$ (in a.u.), as functions of electron momentum q_x (restricted to the x axis only) for the neon atom with $l = 1$ and $m = 1$, obtained using the STO or the asymptotic ground-state wave function. In (a) the red solid line corresponds to the case of STO, while the black dashed line corresponds to the case of asymptotic wave function. In (b), the red lines correspond to the case of STO (solid line for the x and dot-dashed line for the y component), while the black lines correspond to the case of asymptotic wave function (dashed line for the x and dotted line for the y component). (c) shows the vector potential A_x (red dashed line) and the electron momentum q_x (blue solid line), for the solution $(\alpha, \beta, m) = (-1, 1, 0)$ at the moment of recombination, as functions of the harmonic order n. Additionally, in (a) the electron momenta at the moments of recombination for $n = 51$ and $n = 281$ are indicated by blue arrows.

$n = 281$ than for $n = 51$. The difference can also be seen in Fig. 9(b), where we plotted the logarithm of the recombination matrix element (5) as a function of the electron momentum for both ground-state wave functions and for two different polarization axes of the emitted harmonic. In Fig. 5(c) (the inset in the upper right corner) we have also plotted the vector potential A_x (red dashed line) and electron momentum q_x (blue solid line) at the moment of recombination as functions of the harmonic order n for the solution $(\alpha, \beta, m) = (-1, 1, 0)$. The intensity of the electron momentum vector at the moment of recombination increases with the harmonic order n, and this is the reason for the gradual change in the difference of the heights of the two spectra as the harmonic order increases.

IV. CONCLUSIONS

We have presented and applied a modified saddle-point method to high-order above-threshold ionization and high-order harmonic generation processes in a linearly polarized laser field for neon atoms with a ground-state wave function expressed as a linear combination of the Slater-type orbitals. The spectra obtained by this method are compared with the spectra obtained by the usual saddle-point method which is applicable to the asymptotic ground-state wave functions. Both methods are compared separately with the results obtained by numerical integration.

In order to find the transition amplitude of the HATI (HHG) process, one has to solve the five-dimensional integral over the rescattering (recombination) time t, the canonical momentum $\mathbf{k}$ between ionization and rescattering (recombination), and the ionization time t_0. The integrals over t and $\mathbf{k}$ are solved by ordinary SPM, while the integral over the ionization time t_0 requires special care. In the case of asymptotic ground-state wave functions, saddle points t_{0s} overlap with singular points, while for the STO ground-state wave functions the saddle points t_{0s} are in close proximity to singular points t_{0si} (one for each STO). The problem of overlapping saddle and singular points was solved in Ref. [30], and so far the use of asymptotic ground-state wave functions has been a common practice in the SPM treatment of HATI and HHG.

In this paper, we presented a modified SPM applied to HATI and HHG, which treats the proximity problem of the saddle and singular points that arises when we use the STOs as the ground-state wave functions. The idea of the presented method is to expand the part of the T-matrix element responsible for the appearance of singularities in the Laurent series around each of the singular points, and then to integrate the principal and regular parts of the Laurent series separately. The integral over the principal part is related to the complementary error function and is calculated using a recurrence relation, while the regular part is integrated using the ordinary SPM. The algorithm for finding singular points consists of first finding the saddle points $\{t_{0s}, t_s\}$, and then, for each SP solution and each STO, finding the corresponding singular point t_{0si}.

The spectra obtained using our modified SPM are in excellent agreement with those obtained by the numerical integration, for both the HATI and HHG processes. In the case of HATI, the rates obtained using the STO ground-state wave function were slightly lower than those obtained using the

asymptotic ground-state wave function. However, the difference in height between these two spectra remained constant for all electron energies, and there was no other structural difference between the spectra. If we had used more STOs to describe the ground-state wave function, the two spectra would overlap completely. Since the ionization takes place far away from the nucleus, we concluded that in the case of the HATI process it is justified to use either the asymptotic or the STO ground-state wave functions.

In the case of the HHG process, there is also a small difference between the spectra obtained using the asymptotic and STO wave functions, but in this case the difference in height of the two spectra increases with increasing harmonic order. For lower harmonic orders, these two spectra completely coincide, while for higher harmonic orders, especially near the cutoff energy, the two spectra differ significantly. This behavior is also visible for partial contributions of different solutions of the SP equations. We have shown that this difference in the height of the two spectra is due to the recombination matrix element. Electron recombination occurs close to the center of the atom, where the difference between the asymptotic and the STO ground-state wave functions is the largest.

We have performed a more detailed analysis in momentum space and for the most dominant SP solution. The momentum of the electron at the recombination time increases with increasing harmonic order, while the difference between the asymptotic and STO wave functions in momentum space increases with increasing momentum of the electron, and hence the difference in height of the two spectra increases with increasing harmonic order. Since the asymptotic wave functions correctly describe the behavior of the electrons only far from the nucleus, we concluded that in the case of the HHG process the STO ground-state wave functions and the modified SPM should be used.

Furthermore, for understanding and control of strong-field processes it is important to analyze them in the fashion of Feynman path integral and quantum-orbit formalism [22,49,50]. This can be achieved applying the SPM to calculate observables which are expressed in the form of multidimensional integrals. However, singular points of the subintegral matrix elements may prevent direct application of the SPM. These singular points may overlap or be in close proximity to the saddle points. The results presented in our paper show how this problem can be solved. We have applied our method to HATI and HHG and have shown that it is particularly useful for HHG since the HHG recombination matrix element should contain the STOs for which our modified SPM works well.

The three-step model, mentioned in the Introduction, besides the HHG and HATI, can also be applied to other strong-field processes [see Eqs. (1)–(3) in Ref. [50]]. One important example is nonsequential double ionization (see, for example, the review article [51,52]), in which the returned electron is responsible for liberation of the second electron. Since the first step of this process is also the ionization, it is clear that similar singular points of the ionization matrix element, as those considered in our paper, appear. The saddle-point method was applied to nonsequential double ionization in Refs. [53–57].

The method developed in our paper can also be useful in the context of two recently analyzed phenomena in attosecond science: full quantum optical description and quantum electrodynamics effects in intense laser-matter interactions [58–67] and entanglement and decoherence [68–77]. Since the ionization and recombination matrix elements appear also in these cases, our method is even more useful since, in comparison with semiclassical transition amplitudes, additional integrals may appear for such processes (for example, due to quantum statistics of driving light).

ACKNOWLEDGMENTS

We acknowledge support by the Ministry for Science, Higher Education and Youth Canton Sarajevo, Bosnia and Herzegovina.

APPENDIX: DIPOLE MATRIX ELEMENTS

The dipole matrix element $\langle \mathbf{q}|\mathbf{r}|\psi_0\rangle$ can be written as

$$\langle \mathbf{q}|\mathbf{r}|\psi_0\rangle = \frac{1}{(2\pi)^{3/2}} i\frac{\partial}{\partial \mathbf{q}} \int d\mathbf{r} e^{-i\mathbf{q}\cdot\mathbf{r}}\psi_0(\mathbf{r}) = i\frac{\partial}{\partial \mathbf{q}}\tilde{\psi}_0(\mathbf{q}). \tag{A1}$$

Therefore, we need the ground-state wave function in momentum space $\tilde{\psi}_0(\mathbf{q})$. We will separately derive momentum-space wave functions of the neon atom for the case of asymptotic ground-state wave function and for the case of wave function described by a linear combination of STOs.

1. Asymptotic ground-state wave function

Bound-state asymptotic wave function for valence electron of the neon atom is given by [78]

$$\psi_{\nu l\mathrm{m}}(\mathbf{r}) = A r^{\nu-1} e^{-\kappa r} Y_{lm}(\hat{\mathbf{r}}), \quad r \gg 1, \tag{A2}$$

with $\nu = 1/\kappa$, $\kappa = \sqrt{2I_p}$, $A = 2.1$, $l = 1$, and $I_p = 21.56$eV. In order to derive the asymptotic wave function in momentum space

$$\tilde{\psi}_{\nu l\mathrm{m}}(\mathbf{q}) = \frac{1}{(2\pi)^{3/2}} \int d\mathbf{r} e^{-i\mathbf{q}\cdot\mathbf{r}}\psi_{\nu lm}(\mathbf{r}), \tag{A3}$$

we expand the plane wave $\exp(-i\mathbf{q}\cdot\mathbf{r})$ in spherical harmonics

$$e^{-i\mathbf{q}\cdot\mathbf{r}} = 4\pi \sum_{l=0}^{\infty}(-i)^l j_l(qr) \sum_{m=-l}^{l} Y^*_{lm}(\hat{\mathbf{r}})Y_{lm}(\hat{\mathbf{q}}), \tag{A4}$$

where $j_l(qr) = \sqrt{\frac{\pi}{2qr}} J_{l+\frac{1}{2}}(qr)$ are spherical Bessel functions and $Y_{lm}(\hat{\mathbf{q}})$ are spherical harmonics in momentum space. Writing $d\mathbf{r} = r^2 dr d\Omega$, we get

$$\tilde{\psi}_{\nu lm}(\mathbf{q}) = \sqrt{\frac{2}{\pi}} A \int dr\, r^{\nu+1} e^{-\kappa r} \sum_{l'=0}^{\infty} \sum_{m'=-l'}^{l'} (-i)^{l'} \times j_{l'}(qr) Y_{l'm'}(\hat{\mathbf{q}}) \int d\Omega\, Y^*_{l'm'}(\hat{\mathbf{r}}) Y_{lm}(\hat{\mathbf{r}}). \tag{A5}$$

Using the orthonormality condition of spherical harmonics

$$\int d\Omega\, Y^*_{l'm'}(\hat{\mathbf{r}}) Y_{lm}(\hat{\mathbf{r}}) = \delta_{ll'}\,\delta_{mm'}, \tag{A6}$$

Eq. (A5) becomes

$$\tilde{\psi}_{\nu l\mathrm{m}}(\mathbf{q}) = \sqrt{\frac{2}{\pi}} A\,(-i)^l\, Y_{lm}(\hat{\mathbf{q}}) \int dr\, r^{\nu+1} \exp(-\kappa r) j_l(qr). \tag{A7}$$

The integral in Eq. (A7) can be solved using formula (see 6.621 in Ref. [79])

$$\int_0^\infty e^{-\sigma x} J_\lambda(\varepsilon x)\, x^{\mu-1}\, dx = \frac{\left(\frac{\varepsilon}{2\sigma}\right)^\lambda \Gamma(\lambda+\mu)}{\sigma^\mu\, \Gamma(\lambda+1)} \left(1+\frac{\varepsilon^2}{\sigma^2}\right)^{\frac{1}{2}-\mu} {}_2F_1\left(\frac{\lambda-\mu+1}{2}, \frac{\lambda-\mu}{2}+1; \lambda+1; -\frac{\varepsilon^2}{\sigma^2}\right), \tag{A8}$$

where ${}_2F_1(a, b; c; z)$ is the hypergeometric function. We get

$$\tilde{\psi}_{\nu l\mathrm{m}}(\mathbf{q}) = \frac{A}{2^{l+1/2}\,\kappa^{l-\nu}} \frac{\Gamma(l+\nu+2)}{\Gamma(l+3/2)} Y_{lm}(\hat{\mathbf{q}}) f_l(q), \tag{A9}$$

$$f_l(q) = \frac{(-iq)^l}{(q^2+\kappa^2)^{\nu+1}} {}_2F_1\left(\alpha, \beta; \gamma; -\frac{q^2}{\kappa^2}\right), \tag{A10}$$

with $\alpha = (l-\nu)/2$, $\beta = (l-\nu+1)/2$, and $\gamma = l+3/2$, so that the dipole matrix element (A1) becomes

$$\langle \mathbf{q}|\mathbf{r}|\psi_{\nu l\mathrm{m}}\rangle = i \frac{A}{2^{l+1/2}\,\kappa^{l-\nu}} \frac{\Gamma(l+\nu+2)}{\Gamma(l+3/2)} \left[Y_{lm}(\hat{\mathbf{q}}) \frac{\partial f_l(q)}{\partial q} \hat{\mathbf{q}} + f_l(q) \frac{\partial Y_{lm}(\hat{\mathbf{q}})}{\partial \mathbf{q}} \right]. \tag{A11}$$

Using the formula

$$\frac{\partial\, {}_2F_1(\alpha, \beta; \gamma; z)}{\partial z} = \frac{\alpha\beta}{\gamma} {}_2F_1(\alpha+1, \beta+1; \gamma+1; z), \tag{A12}$$

we get

$$\frac{\partial f_l(q)}{\partial q} = -i \frac{(-iq)^{l-1}}{(q^2+\kappa^2)^{\nu+1}} \left\{ \left[l - 2(\nu+1)\frac{q^2}{q^2+\kappa^2} \right] {}_2F_1\left(\alpha, \beta; \gamma; -\frac{q^2}{\kappa^2}\right) - \frac{2\alpha\beta}{\gamma} \frac{q^2}{\kappa^2} {}_2F_1\left(\alpha+1, \beta+1; \gamma+1; -\frac{q^2}{\kappa^2}\right) \right\}. \tag{A13}$$

Also, for $l = 1$ and $m = \pm 1$ spherical harmonics and their gradients (in momentum space) are given by

$$Y_{1m}(\hat{\mathbf{q}}) = -m \sqrt{\frac{3}{8\pi}} \frac{q_x + i m q_y}{q} \tag{A14}$$

and

$$\frac{\partial Y_{1m}(\hat{\mathbf{q}})}{\partial \mathbf{q}} = -m \sqrt{\frac{3}{8\pi}} \frac{1}{\left(q_x^2+q_y^2\right)^{3/2}} \left[\left(q_y^2 - i m q_x q_y\right) \hat{\mathbf{e}}_x + \left(i m q_x^2 - q_x q_y\right) \hat{\mathbf{e}}_y \right]. \tag{A15}$$

2. Slater-type-orbital ground-state wave function

Bound state of the valence electron of the neon atom, which is in the $2p$ state ($n = 2$, $l = 1$), can be more precisely expressed as a linear combination of four STOs [47],

$$\psi_{21m}(\mathbf{r}) = \frac{2}{\sqrt{3}} \sum_{i=1}^{4} C_i \zeta_i^{5/2} r e^{-\zeta_i r} Y_{1m}(\hat{\mathbf{r}}), \tag{A16}$$

with $C_i = \{0.2180, 0.5334, 0.3293, 0.0187\}$ a.u. and $\zeta_i = \{1.4521, 2.3817, 4.4849, 9.1346\}$ a.u. It can be noticed that STOs for $n = 2$ and $l = 1$ have the same form as asymptotic wave function (A2) with ν replaced by 2, κ replaced by ζ_i, and A replaced by $\frac{2}{\sqrt{3}} C_i \zeta_i^{5/2}$. Therefore, comparing with Eq. (A9), we get

$$\tilde{\psi}_{21m}(\mathbf{q}) = -i \frac{q}{\sqrt{6}} \frac{\Gamma(5)}{\Gamma(5/2)} Y_{1m}(\hat{\mathbf{q}}) \sum_{i=1}^{4} C_i \zeta_i^{7/2} \frac{1}{\left(q^2+\zeta_i^2\right)^3} {}_2F_1\left(-\frac{1}{2}, 0; \frac{5}{2}; -\frac{q^2}{\zeta_i^2}\right). \tag{A17}$$

Since ${}_2F_1(a, 0; c; z) = 1$, for the momentum space ground wave function we obtain

$$\tilde{\psi}_{21m}(\mathbf{q}) = 16 \sqrt{\frac{2}{3\pi}} C_i \zeta_i^{7/2} Y_{1m}(\hat{\mathbf{q}}) \frac{-iq}{\left(q^2+\zeta_i^2\right)^3}. \tag{A18}$$

Inserting Eq. (A14) and calculating the momentum gradient, the dipole matrix element (A1) for the neon atom and $m = \pm 1$ becomes

$$\langle \mathbf{q}|\mathbf{r}|\psi_{21m}\rangle = -m\sum_{i=1}^{4} C_i \frac{8\zeta_i^{7/2}}{\pi}\frac{1}{\left(q^2+\zeta_i^2\right)^4}\left[\left(q^2-6q_x^2-6miq_xq_y+\zeta_i^2\right)\hat{\mathbf{e}}_x+\left(miq^2-6q_xq_y-6miq_y^2+mi\zeta_i^2\right)\hat{\mathbf{e}}_y\right]. \quad \text{(A19)}$$

[1] A. Scrinzi, M. Yu. Ivanov, R. Kienberger, and D. M. Villeneuve, Attosecond physics, J. Phys. B **39**, R1 (2006).

[2] D. B. Milošević, G. G. Paulus, D. Bauer, and W. Becker, Above-threshold ionization by few-cycle pulses, J. Phys. B **39**, R203 (2006).

[3] F. Krausz and M. Ivanov, Attosecond physics, Rev. Mod. Phys. **81**, 163 (2009).

[4] M. Nisoli and G. Sansone, New frontiers in attosecond science, Prog. Quantum Electron. **33**, 17 (2009).

[5] Z. Chang, *Fundamentals of Attosecond Optics* (CRC Press, Boca Raton, 2011).

[6] W. Becker, F. Grasbon, R. Kopold, D. B. Milošević, G. G. Paulus, and H. Walther, Above-threshold ionization: From classical features to quantum effects, Adv. At. Mol. Opt. Phys. **48**, 35 (2002).

[7] C. D. Lin, A. T. Le, Z. Chen, T. Morishita, and R. Lucchese, Strong-field rescattering physics-self-imaging of a molecule by its own electrons, J. Phys. B **43**, 122001 (2010).

[8] P. Agostini and L. F. DiMauro, Atomic and molecular ionization dynamics in strong laser fields: From optical to x-rays, Adv. At. Mol. Opt. Phys. **61**, 117 (2012).

[9] C. Figueira de Morisson Faria and A. S. Maxwell, It is all about phases: Ultrafast holographic photoelectron imaging, Rep. Prog. Phys. **83**, 034401 (2020).

[10] P. Salières, A. L'Huillier, P. Antoine, and M. Lewenstein, Study of the spatial and temporal coherence of high-order harmonics, Adv. At. Mol. Opt. Phys. **41**, 83 (1999).

[11] M. C. Kohler, T. Pfeifer, K. Z. Hatsagortsyan, and C. H. Keitel, Frontiers of atomic high-harmonic generation, Adv. At. Mol. Opt. Phys. **61**, 159 (2012).

[12] A. Nayak *et al.*, Saddle point approaches in strong field physics and generation of attosecond pulses, Phys. Rep. **833**, 1 (2019).

[13] P. B. Corkum, Plasma perspective on strong field multiphoton ionization, Phys. Rev. Lett. **71**, 1994 (1993).

[14] K. J. Schafer, B. Yang, L. F. DiMauro, and K. C. Kulander, Above threshold ionization beyond the high harmonic cutoff, Phys. Rev. Lett. **70**, 1599 (1993).

[15] M. Lewenstein, Ph. Balcou, M. Yu. Ivanov, Anne L'Huillier, and P. B. Corkum, Theory of high-harmonic generation by low-frequency laser fields, Phys. Rev. A **49**, 2117 (1994).

[16] M. Lewenstein, K. C. Kulander, K. J. Schafer, and P. H. Bucksbaum, Rings in above-threshold ionization: A quasiclassical analysis, Phys. Rev. A **51**, 1495 (1995).

[17] K. Amini, J. Biegert, F. Calegari, A. Chacón, M. F. Ciappina, A. Dauphin, D. K. Efimov, C. Figueira de Morisson Faria, K. Giergiel, P. Gniewek, and A. S. Landsman, Symphony on strong field approximation, Rep. Prog. Phys. **82**, 116001 (2019).

[18] A. Jašarević, E. Hasović, R. Kopold, W. Becker, and D. B. Milošević, Application of the saddle-point method to strong-laser-field ionization, J. Phys. A: Math. Theor. **53**, 125201 (2020).

[19] D. B. Milošević and W. Becker, Role of long quantum orbits in high-order harmonic generation, Phys. Rev. A **66**, 063417 (2002).

[20] D. B. Milošević, E. Hasović, M. Busuladžić, A. Gazibegović-Busuladžić, and W. Becker, Intensity-dependent enhancements in high-order above-threshold ionization, Phys. Rev. A **76**, 053410 (2007).

[21] D. B. Milošević, Forward- and backward-scattering quantum orbits in above-threshold ionization, Phys. Rev. A **90**, 063414 (2014).

[22] R. Kopold, D. B. Milošević, and W. Becker, Rescattering processes for elliptical polarization: A quantum trajectory analysis, Phys. Rev. Lett. **84**, 3831 (2000).

[23] X.-Y. Lai, C.-L. Wang, Y.-J. Chen, Z.-L. Hu, W. Quan, X.-J. Liu, J. Chen, Y. Cheng, Z.-Z. Xu, and W. Becker, Elliptical polarization favors long quantum orbits in high-order above-threshold ionization of noble gases, Phys. Rev. Lett. **110**, 043002 (2013).

[24] W. Quan, X.-Y. Lai, Y.-J. Chen, C.-L. Wang, Z.-L. Hu, X.-J. Liu, X.-L. Hao, J. Chen, E. Hasović, M. Busuladžić, D. B. Milošević, and W. Becker, Quantum orbits: A powerful concept in laser-atom physics, Chin. J. Phys. **52**, 389 (2014).

[25] D. B. Milošević, W. Becker, and R. Kopold, Generation of circularly polarized high-order harmonics by two-color coplanar field mixing, Phys. Rev. A **61**, 063403 (2000).

[26] D. B. Milošević and W. Becker, Improved strong-field approximation and quantum-orbit theory: Application to ionization by a bicircular laser field, Phys. Rev. A **93**, 063418 (2016).

[27] D. B. Milošević, Quantum-orbit analysis of high-order harmonic generation by bicircular field, J. Mod. Opt. **66**, 47 (2019).

[28] D. B. Milošević and W. Becker, X-ray harmonic generation by orthogonally polarized two-color fields: Spectral shape and polarization, Phys. Rev. A **100**, 031401(R) (2019).

[29] A. S. Jašarević, E. Hasović, and D. B. Milošević, Ionization by a strong orthogonal two-color laser field: A quantum-orbit-theory approach, Eur. Phys. J. D **76**, 239 (2022).

[30] G. F. Gribakin and M. Yu. Kuchiev, Multiphoton detachment of electrons from negative ions, Phys. Rev. A **55**, 3760 (1997).

[31] A. S. Jašarević, E. Hasović, and D. B. Milošević, Modified saddle-point method applied to direct ionization of noble gas atoms, J. Phys. A: Math. Theor. **56**, 335201 (2023).

[32] A. E. S. Green, D. E. Rio, and T. Ueda, Analytic velocity-dependent potential for bound and scattering states of electrons and atoms, Phys. Rev. A **24**, 3010 (1981).

[33] D. B. Milošević, Circularly polarized high harmonics generated by a bicircular field from inert atomic gases in the p state: A tool for exploring chirality-sensitive processes, Phys. Rev. A **92**, 043827 (2015).

[34] N. Bleistein and R. A. Handelsman, *Asymptotic Expansions of Integrals* (Dover, New York, 1986).
[35] R. Wong, *Asymptotic Approximations of Integrals* (Academic, New York, 1989).
[36] V. A. Borovikov, *Uniform Stationary Phase Method* (The Institution of Electrical Engineers, London, 1994).
[37] P. D. Miller, *Applied Asymptotic Analysis* (American Mathematical Society, Providence, 2006).
[38] N. G. de Bruijn, *Asymptotic Methods in Analysis* (Dover, New York, 2010).
[39] N. M. Temme, *Asymptotic Methods for Integrals*, Series in Analysis, Vol. 6 (World Scientific, Singapore, 2015).
[40] V. N. Ostrovsky and J. B. Greenwood, High harmonic generation by halogen anions and noble gas atoms in a laser field, J. Phys. B **38**, 1867 (2005).
[41] V. N. Ostrovsky, High harmonic generation by anions and atoms: Effect of initial/final-state wave functions, J. Phys. B **38**, 4399 (2005).
[42] B. Fetić, D. B. Milošević, and W. Becker, High-order above-threshold ionisation of atoms and negative ions: Channel-closing effects and the low-frequency approximation, J. Mod. Opt. **58**, 1149 (2011).
[43] T. K. Kjeldsen and L. B. Madsen, Strong-field ionization of atoms and molecules: The two-term saddle-point method, Phys. Rev. A **74**, 023407 (2006).
[44] S. F. C. Shearer, M. C. Smyth, and G. F. Gribakin, Electron detachment from negative ions in a short laser pulse, Phys. Rev. A **84**, 033409 (2011).
[45] S. V. Popruzhenko, Ph. A. Korneev, S. P. Goreslavski, and W. Becker, Laser-induced recollision phenomena: Interference resonances at channel closings, Phys. Rev. Lett. **89**, 023001 (2002).
[46] C. Figueira de Morisson Faria, H. Schomerus, and W. Becker, High-order above-threshold ionization: The uniform approximation and the effect of the binding potential, Phys. Rev. A **66**, 043413 (2002).
[47] A. A. Radzig and B. M. Smirnov, *Reference Data on Atoms, Molecules and Ions* (Springer, Berlin, 1985).
[48] C. F. Bunge, J. A. Barrientos, and A. V. Bunge, At. Data Nucl. Data Tables **53**, 113 (1993).
[49] P. Salières, B. Carré, L. Le Déroff, F. Grasbon, G. G. Paulus, H. Walther, R. Kopold, W. Becker, D. B. Milošević, A. Sanpera, and M. Lewenstein, Feynman's path-integral approach for intense-laser-atom interactions, Science **292**, 902 (2001).
[50] D. B. Milošević, D. Bauer, and W. Becker, Quantum-orbit theory of high-order atomic processes in intense laser fields, J. Mod. Opt. **53**, 125 (2006).
[51] C. Figueira de Morisson Faria and X. Liu, Electron-electron correlation in strong laser fields, J. Mod. Opt. **58**, 1076 (2011).
[52] W. Becker, X. Liu, P. J. Ho, and J. H. Eberly, Theories of photoelectron correlation in laser-driven multiple atomic ionization, Rev. Mod. Phys. **84**, 1011 (2012).
[53] T. Shaaran and C. Figueira de Morisson Faria, Laser-induced nonsequential double ionization: Kinematic constraints for the recollision-excitation-tunneling mechanism, J. Mod. Opt. **57**, 984 (2010).
[54] T. Shaaran, M. T. Nygren, and C. Figueira de Morisson Faria, Laser-induced nonsequential double ionization at and above the recollision-excitation-tunneling threshold, Phys. Rev. A **81**, 063413 (2010).
[55] T. Shaaran, C. Figueira de Morisson Faria, and H. Schomerus, Causality and quantum interference in time-delayed laser-induced nonsequential double ionization, Phys. Rev. A **85**, 023423 (2012).
[56] A. S. Maxwell and C. Figueira de Morisson Faria, Quantum interference in time-delayed nonsequential double ionization, Phys. Rev. A **92**, 023421 (2015).
[57] A. S. Maxwell and C. Figueira de Morisson Faria, Controlling below-threshold nonsequential double ionization via quantum interference, Phys. Rev. Lett. **116**, 143001 (2016).
[58] A. Gorlach, O. Neufeld, N. Rivera, O. Cohen, and I. Kaminer, The quantum-optical nature of high harmonic generation, Nat. Commun. **11**, 4598 (2020).
[59] M. Lewenstein, M. F. Ciappina, E. Pisanty, J. Rivera-Dean, P. Stammer, Th. Lamprou, and P. Tzallas, Generation of optical Schrödinger cat states in intense laser-matter interactions, Nat. Phys. **17**, 1104 (2021).
[60] J. Rivera-Dean, P. Stammer, A. S. Maxwell, Th. Lamprou, P. Tzallas, M. Lewenstein, and M. F. Ciappina, Light-matter entanglement after above-threshold ionization processes in atoms, Phys. Rev. A **106**, 063705 (2022).
[61] P. Stammer, J. Rivera-Dean, A. Maxwell, Th. Lamprou, A. Ordóñez, M. F. Ciappina, P. Tzallas, and M. Lewenstein, Quantum electrodynamics of intense laser-matter interactions: A tool for quantum state engineering, PRX Quantum **4**, 010201 (2023).
[62] U. Bhattacharya, Th. Lamprou, A. S. Maxwell, A. Ordóñez, E. Pisanty, J. Rivera-Dean, P. Stammer, M. F. Ciappina, M. Lewenstein, and P. Tzallas, Strong-laser-field physics, non-classical light states and quantum information science, Rep. Prog. Phys. **86**, 094401 (2023).
[63] D. B. Milošević, Quantum theory of photon emission during strong-laser-field-induced ionization, Phys. Rev. A **108**, 033110 (2023).
[64] M. E. Tzur, M. Birk, A. Gorlach, M. Krüger, I. Kaminer, and O. Cohen, Photon-statistics force in ultrafast electron dynamics, Nat. Photon. **17**, 501 (2023).
[65] Y. Fang, F.-X. Sun, Q. He, and Y. Liu, Strong-field ionization of hydrogen atoms with quantum light, Phys. Rev. Lett. **130**, 253201 (2023).
[66] A. Gorlach, M. E. Tzur, M. Birk, M. Krüger, N. Rivera, O. Cohen, and I. Kaminer, High-harmonic generation driven by quantum light, Nat. Phys. **19**, 1689 (2023).
[67] S. Yi, I. Babushkin, O. Smirnova, and M. Ivanov, Generation of massively entangled bright states of light during harmonic generation in resonant media, arXiv:2401.02817.
[68] T. Nishi, E. Lötstedt, and K. Yamanouchi, Entanglement and coherence in photoionization of H_2 by an ultrashort XUV laser pulse, Phys. Rev. A **100**, 013421 (2019).
[69] M. J. J. Vrakking, Control of attosecond entanglement and coherence, Phys. Rev. Lett. **126**, 113203 (2021).
[70] M. J. J. Vrakking, Ion-photoelectron entanglement in photoionization with chirped laser pulses, J. Phys. B **55**, 134001 (2022).
[71] L.-M. Koll, L. Maikowski, L. Drescher, T. Witting, and M. J. J. Vrakking, Experimental control of quantum-mechanical entanglement in an attosecond pump-probe experiment, Phys. Rev. Lett. **128**, 043201 (2022).

[72] A. S. Maxwell, L. B. Madsen, and M. Lewenstein, Entanglement of orbital angular momentum in non-sequential double ionization, Nat. Commun. **13**, 4706 (2022).

[73] D. Busto, H. Laurell, D. Finkelstein-Shapiro, Ch. Alexandridi, M. Isinger, S. Nandi, R. J. Squibb, M. Turconi, S. Zhong, C. L. Arnold, R. Feifel, M. Gisselbrecht, P. Salières, T. Pullerits, F. Martin, L. Argenti, and A. L'Huillier, Probing electronic decoherence with high-resolution attosecond photoelectron interferometry, Eur. Phys. J. D **76**, 112 (2022).

[74] H. Laurell, D. Finkelstein-Shapiro, C. Dittel, C. Guo, R. Demjaha, M. Ammitzböll, R. Weissenbilder, L. Neoričić, S. Luo, M. Gisselbrecht, C. L. Arnold, A. Buchleitner, T. Pullerits, A. L'Huillier, and D. Busto, Continuous-variable quantum state tomography of photoelectrons, Phys. Rev. Res. **4**, 033220 (2022).

[75] Y. Nabekawa and K. Midorikawa, Analysis of attosecond entanglement and coherence using feasible formulae, Phys. Rev. Res. **5**, 033083 (2023).

[76] M. Lewenstein, N. Baldelli, U. Bhattacharya, J. Biegert, M. F. Ciappina, T. Grass, P. T. Grochowski, A. S. Johnson, Th. Lamprou, A. S. Maxwell, A. Ordóñez, E. Pisanty, J. Rivera-Dean, P. Stammer, and P. Tzallas, *Attosecond Physics and Quantum Information Science*, in Proceedings of the 8th International Conference on Attosecond Science and Technology (ATTO 2023); Springer Proceedings in Physics, edited by L. Argenti *et al.* (Springer Nature, New York, 2024), Vol. 300.

[77] M. Ruberti, V. Averbukh, and F. Mintert, Bell test of quantum entanglement in attosecond photoionization, arXiv:2312.05036.

[78] B. M. Smirnov, *Physics of Atoms and Ions* (Springer, New York, 2003).

[79] I. S. Gradshtein and I. M. Ryzhik, *Tables of Integrals, Series, and Products*, 7th ed. (Academic, New York, 2007).